FATIGUE AND CORROSION FATIGUE OF 8090 Al-Li-Cu-Mg ALLOY

F. Haddleton, S. Murphy, T. Griffin

JOURNAL DE PHYSIQUE
Colloque C3, supplément au n°9, Tome 48, septembre 1987

FATIGUE AND CORROSION FATIGUE OF 8090 Al-Li-Cu-Mg ALLOY

F.L. HADDLETON, S. MURPHY and T.J. GRIFFIN*

Department of Mechanical and Production Engineering, Aston University, Aston Triangle, Gosta Green, GB-Birmingham B4 7ET Great-Britain
**Dunlop Ltd., Aviation Division, GB-Coventry, Great-Britain*

Abstract

The fatigue resistance of metals can be profoundly affected by the environmental reactions that change crack initiation and propagation processes. These corrosion fatigue processes can occur in high strength aluminium alloys in aircraft, which frequently encounter salt spray and high humidity environments. For this reason, the fatigue behaviour of 8090-T6 alloy in the form of 25mm thick plate has been investigated in both air and an aerated 2.5% NaCl solution. Results are compared to a conventional high strength aluminium alloy, 2014-T6.

Fatigue crack initiation and propagation data are presented for different crack orientations and mean stress levels. The slightly lower fatigue strength of 8090-T6 in air is attributed to earlier crack initiation. The fatigue crack propagation behaviour of 8090-T6 is shown to be superior to that of 2014-T6 at low to intermediate levels of ΔK, under both environmental conditions. The mechanisms associated with fatigue crack initiation and propagation, and environmental effects, are discussed.

Introduction

The replacement of conventional high strength aluminium alloys in airframe applications with recently developed aluminium-lithium based alloys has been shown to offer weight savings, due to the increase in specific properties that result from the decrease in density and increase in modulus (1).

Work has concentrated on the development of alloys to meet the property levels of conventional high strength aluminium alloys. A series of three Al-Li-Cu-Mg alloys has been developed to meet these requirements (2,3). Improved alloy chemistry and manufacturing techniques in the last few years have made this possible. The combination of these properties and the resultant 10% lower density and 10% higher modulus than conventional aluminium alloys make these Al-Li-Cu-Mg alloys attractive for airframe applications.

The fatigue performances of aluminium-lithium based alloys have been shown to be superior to conventional alloys, with crack growth resistance far better at low levels of ΔK (2,4). Although fatigue, corrosion and SCC properties of Al-Li-Cu-Mg alloys have been investigated (4,5,6), little attention has been given to their corrosion fatigue properties The aim of this work was to investigate the fatigue and corrosion fatigue properties of one of these alloys, and compare with a conventional 2XXX series aluminium alloy.

Experimental Procedure

The material under investigation was alloy 8090 (2,3), in the form of 25mm thick rolled plate supplied by Alcan International Ltd. and RAE. The chemical composition of the alloy was (wt.%): 2.50Li - 1.19Cu - 0.67Mg - 0.10Zr.

The material was supplied in the T8 condition, where a 2.5% cold stretch was given in between solution treatment and artificial ageing. However, for the applications that the authors are concerned with a stretching treatment was impracticable. A further heat treatment was therefore carried out to provide a T6 temper, a solution treated and artificially aged condition. Solution heat treatment was carried out at 530°C for one hour, followed by a cold water quench. The ageing treatment was carried out at 190°C for 24 hours. Comparative tests were performed on BS L168, conforming to 2014-T6.

Tensile tests were performed on 2014-T6 and 8090 in both the T6 and T8 conditions in order to quantify the reduction in tensile properties resulting from the lack of a cold stretch. Tests were carried out in both the longitudinal (L) and transverse (T) directions, with at least two tests performed for each condition.

Fatigue testing was carried out on two different types of specimen. For fatigue life testing, rotating beam specimens were used, where R=-1.0 (R is the ratio of minimum to maximum stress). The notched specimens were longitudinally oriented with relation to the rolling direction in the case of both 8090 and 2014, with a stress concentration factor, K_t, of 1.02. An Avery Dynamic fatigue testing machine was used, with a frequency of 50Hz. For corrosion fatigue life testing, a weeping wick arrangement was used to create a salt water environment from a 3.5% NaCl solution supply.

Fatigue crack initiation testing was performed on notched 4-point bend specimens with a K_t of 1.50, using a Servotest 50kN electrohydraulic machine. The 8090 alloy was tested in three directions, L-S, L-T and T-L, with 2014 in the L-S direction, and an R-value of 0.45 was used throughout.

Fatigue crack propagation tests were carried out on three-point bend specimens, on the same machine. The same crack orientations, L-S, L-T and T-L, were investigated, with R-values of 0.1 and 0.45. 8090 specimens tested in the L-S direction had to be side-grooved in order to produce propagation data. 5% side-grooving was sufficient to stop the crack branching off perpendicular to the intended direction, as shown in Figure 1. For corrosion fatigue initiation and propagation testing the specimens were immersed in an aerated 3.5% NaCl solution, and a frequency of 10Hz was used. The initiation and propagation of fatigue cracks were monitored by the potential drop technique.

Optical and SEM techniques were used to characterize the microstructures of the fracture surfaces.

Results

The results of the tensile testing are shown in Table I, along with typical values for 8090-T8 for comparison (7). The T8 condition was shown to be typical of 8090 in plate form. In general, the T8 condition gave superior tensile properties when compared to the T6 condition, although the ductility appeared unchanged.

The results of the fatigue life tests are shown in Figure 2, for both 8090-T6 and 2014-T6. They are presented in the form of S-N curves, peak stress plotted versus cycles to failure, N_f, for both laboratory air and a 3.5% NaCl solution environment. In general the fatigue life of 2014-T6 exceeded that of 8090-T6 at all stresses except close to the fatigue limit in both air and salt water.

Fatigue crack initiation results are presented in Figure 3, for both laboratory air and 3.5% NaCl solution, in the form of S-N curves where peak stress is plotted against cycles to initiation, N_i. Again, the fatigue crack initiation life of 2014-T6 in air exceeded that of 8090-T6 at high stresses, with similar fatigue lives close to the fatigue limit. This effect was not as pronounced in a salt water environment, where 8090-T6 was superior to 2014-T6 at stresses close to the fatigue limit.

Fatigue crack propagation data is presented in Figure 4, plotted as fatigue crack propagation rate, da/dN, versus cyclic stress intensity factor, ΔK. Results are presented for 8090-T6 and 2014-T6 in both laboratory air and 3.5% NaCl solution. In air the fatigue crack propagation resistance for 8090-T6 was superior to that of 2014-T6, markedly so at low levels of ΔK. At high levels of ΔK, fatigue crack growth rates were similar for both materials. In a salt water environment fatigue crack growth resistance was more dependent upon crack orientation for 8090-T6. Specimens orientated in the L-S direction showed similar trends to those for laboratory air environments when compared to 2014-T6, with superior fatigue crack growth resistance at low levels of ΔK and similar propagation rates at high levels.

	Test Direction	0.2% PS (MPa)	UTS (MPa)	El (%)
8090-T8 (typical) (7)	L	450	500	5.5
	T	425	485	6.5
8090-T8	L	450	519	5.4
	T	426	497	6.6
8090-T6	L	345	442	6.0
	T	369	458	6.5
2014-T6	L	481	526	10.0

Table I: Tensile properties of 2014 and 8090 in different temper conditions.

However, specimens orientated in the T-L direction showed inferior fatigue crack growth resistance to in salt water at high levels of ΔK and only similar propagation rates at low levels of stress. The response of specimens orientated in the L-T direction in salt water was superior to 2014-T6 at low levels of ΔK but inferior at high levels, the cross-over point depending upon the R-ratio.

Fracture surfaces of the rotating beam specimens are shown in Figure 5, where crack growth directions are seen to be different with 2014, Figure 5a, and 8090, Figure 5b. SEM examination, Figure 6, shows the types of failure involved with 8090, a combination of delamination of longitudinal grain boundaries, Figure 6a, and transgranular failure, Figure 6b. A typical fracture surface for crack propagation specimens can be seen in Figure 7, showing a highly faceted crack path.

Discussion and Conclusions

The fatigue life tests, Figure 2, show that 2014-T6 offered better fatigue resistance than 8090-T6 at all but low levels of stress, close to the fatigue limit. Similar trends were shown with the fatigue crack initiation results in air, Figure 3a, with superiority being more pronounced at higher stresses. However, fatigue crack propagation rates in air were slower in 8090 than 2014, especially at low levels of ΔK, Figure 4. The lower levels of fatigue resistance in air could therefore be partly attributed to poorer fatigue crack initiation properties. Similar observations have been made (4), suggesting that the combination of planar slip and a strong crystallographic texture would lead to early crack nucleation.

The fatigue crack initiation resistance of 8090 was better than or equivalent to 2014 in salt water, Figure 3b, so early initiation is not the cause of the lower fatigue life of 8090 in this corrosive environment. The fatigue crack propagation resistance of 8090 was only clearly superior in the L-S direction in salt water, Figure 4. In the L-T orientation, the fatigue crack propagation resistance of 8090 was only superior to 2014 at low levels of ΔK and the T-L orientation had only equivalent crack growth rates at low levels of stress intensity. It would therefore seem that the poorer corrosion fatigue crack propagation resistance of 8090 plays a part in the reduction of fatigue resistance in salt water.

The difference in crack growth direction also seems to have affected the fatigue lives of the two materials in rotary bending. Early testing indicated that fatigue cracks preferred to propagate along longitudinally aligned grain boundaries in L-S specimens, Figure 1, which may give rise to inferior fatigue crack growth performance if gross delamination occurs. The results of the fatigue life tests, Figure 2, would appear to support this observation.Figure 5 shows the transversely oriented crack growth in 2014, Figure 5a, and the mixture of longitudinal and short transverse crack propagation directions in 8090, Figure 5b, in these longitudinally-oriented specimens. The failure in the 8090 specimens was a combination of delamination of longitudinal grain boundaries, Figure 6a, and transgranular failure, Figure 6b. The faster crack propagation associated with this longitudinal delamination would reduce the fatigue life of 8090 when compared to 2014.

Whereas the fatigue crack initiation resistance of 8090 was inferior to 2014 in air, it was shown to be superior in salt water, Figure 3a and 3b. The most likely reason for the higher drop in fatigue crack initiation resistance of 2014 due to the corrosive environment is the greater amount of pitting corrosion found with this alloy when compared to 8090. Similar observations on the pitting corrosion of 2014 and 8090 have been made (5). Corrosion pits can reduce fatigue crack initiation resistance, and so fatigue life, by introducing stress concentrations at their base.

The crack propagation data for 8090 and 2014 in air, Figure 4, are comparable with published data (2,4),with 8090 being superior at all but high levels of ΔK. The slightly better fatigue crack propagation resistance of the 8090 alloy in this investigation with most published data (2,4) may be due to the larger grain size. Similar results have been obtained (8), showing that the improvement in fatigue properties with increasing grain size can be attributed to a highly faceted crack path, as shown in Figure 7 for the alloy under investigation. Crack closure effects or crack deflection are therefore the possible cause of increased crack growth resistance.

The fatigue crack propagation rates for 8090 did not show the same superiority over 2014 in a salt water environment as they did in air, Figure 4. There are several possible explanations for this. It has been

shown that planar bands of intense slip, caused in aluminium-lithium alloys by the coherent shearable δ' precipitates, are more sensitive to localised corrosion (9). However, positive evidence of this could not be found during electron microscopy studies. Another possible explanation is the occurrence of hydrogen embrittlement ahead of the crack tip, which has been shown to occur in 8090 (6), and was suggested as a possible stress corrosion mechanism. However, this mechanism would only be seen at low frequencies, and the stress corrosion resistance of 8090 has also been shown to be equivalent to or better than 2014 (5,6). The build-up of lithium-ion concentration in the electrolyte within the crack is another possibility for the reduction of fatigue crack resistance of 8090 in a salt water environment, and would also explain the absence of a corresponding reduction in corrosion fatigue crack initiation resistance. Dissolution processes are accelerated by an increase in lithium ion concentration (6), as may occur in the salt water solution close to the tip of a fatigue crack. Lithium ion concentration would not increase noticeably in the aerated bulk solution, so fatigue crack initiation would not be affected.

The propagation of fatigue cracks in aluminium-lithium alloys is clearly complex. Detailed examination of the mechanisms of propagation in air and a corrosive environment is beyond the scope of this paper and requires further study.

Acknowledgements

This work has been carried out with the financial support of the Science and Engineering Research Council (SERC) and Dunlop Aviation Ltd. Thanks are also extended to Prof.J.T.Barnby for his supervision of the project.

References

1. D.Little, in "3rd Int. Conf. on Al-Li Alloys", Inst. of Metals (1986), pp.15-21.

2. C.J.Peel, B.Evans, C.A.Baker, D.A.Bennett, P.J.Gregson, H.M.Flower, in "2nd Int. Conf. on Al-Li Alloys", AIME (1984), pp.363-392.

3. C.J.Peel, B.Evans, D.McDarmaid, in "3rd Int. Conf. on Al-Li Alloys", Inst. of Metals (1986), pp.26-36.

4. M.Peters, K.Welpmann, W.Zink, T.H.Sanders Jr., in "3rd Int. Conf. on Al-Li Alloys", Inst. of Metals (1986), pp.239-246.

5. P.L.Lane, J.A.Gray, C.J.E.Smith, in "3rd Int. Conf. on Al-Li Alloys", Inst. of Metals (1986), pp.273-281.

6. N.J.H.Holroyd, A.Gray, G.M.Scamans, R.Hermann, in "3rd Int. Conf. on Al-Li Alloys", Inst. of Metals (1986), pp.310-320.

7. M.A.Reynolds, A.Gray, E.Creed, R.M.Jordan, A.P.Titchener, in "3rd Int. Conf. on Al-Li Alloys", Inst. of Metals (1986), pp.57-65.

8. S.J.Harris, B.Noble, K.Dinsdale, in "Aluminium Technology '86", Inst. of Metals (1986), pp.451-458.

9. E.A.Starke, Jr., G.Lutjering, in "Fatigue and Microstructure", ASM (1979), pp.205-243.

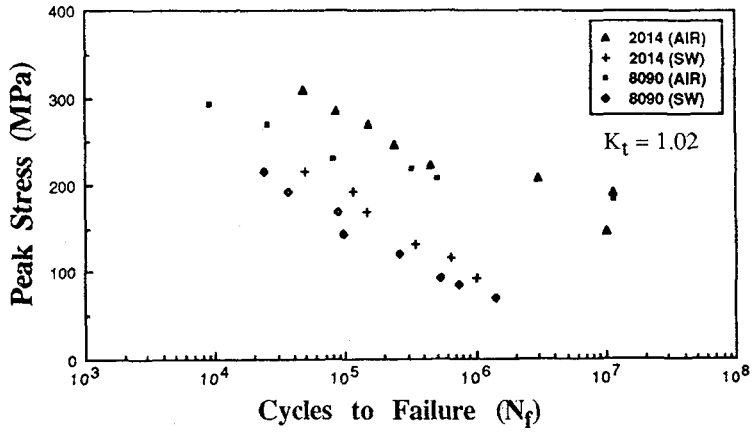

Figure 2: Fatigue life curves for 8090-T6 and 2014-T6 in laboratory air and 3.5% NaCl solution.

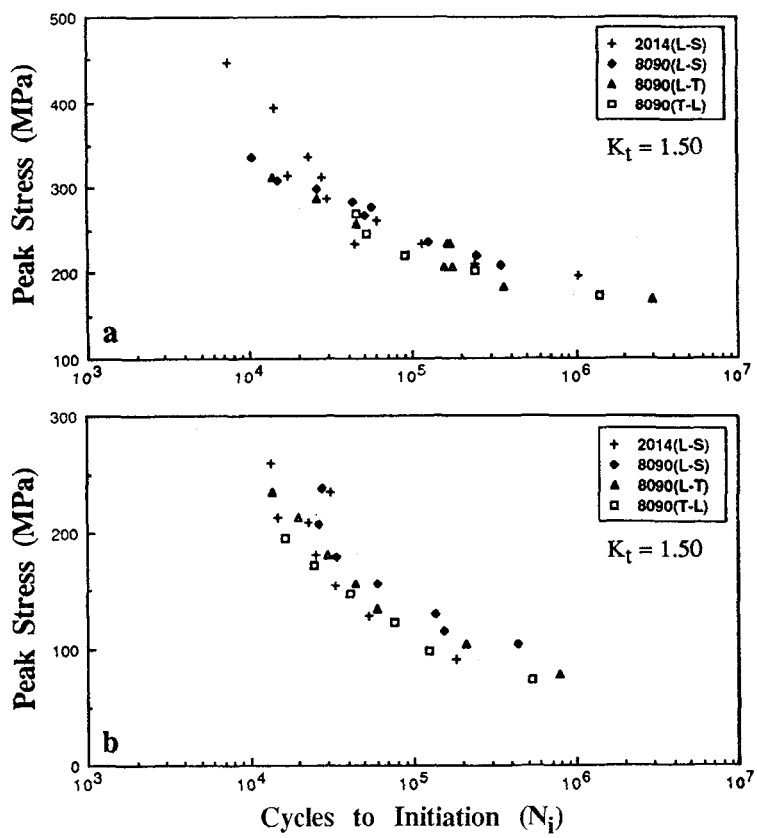

Figure 3: Fatigue crack initiation curves for 8090-T6 and 2014-T6 in laboratory air (a) and 3.5% NaCl solution (b).

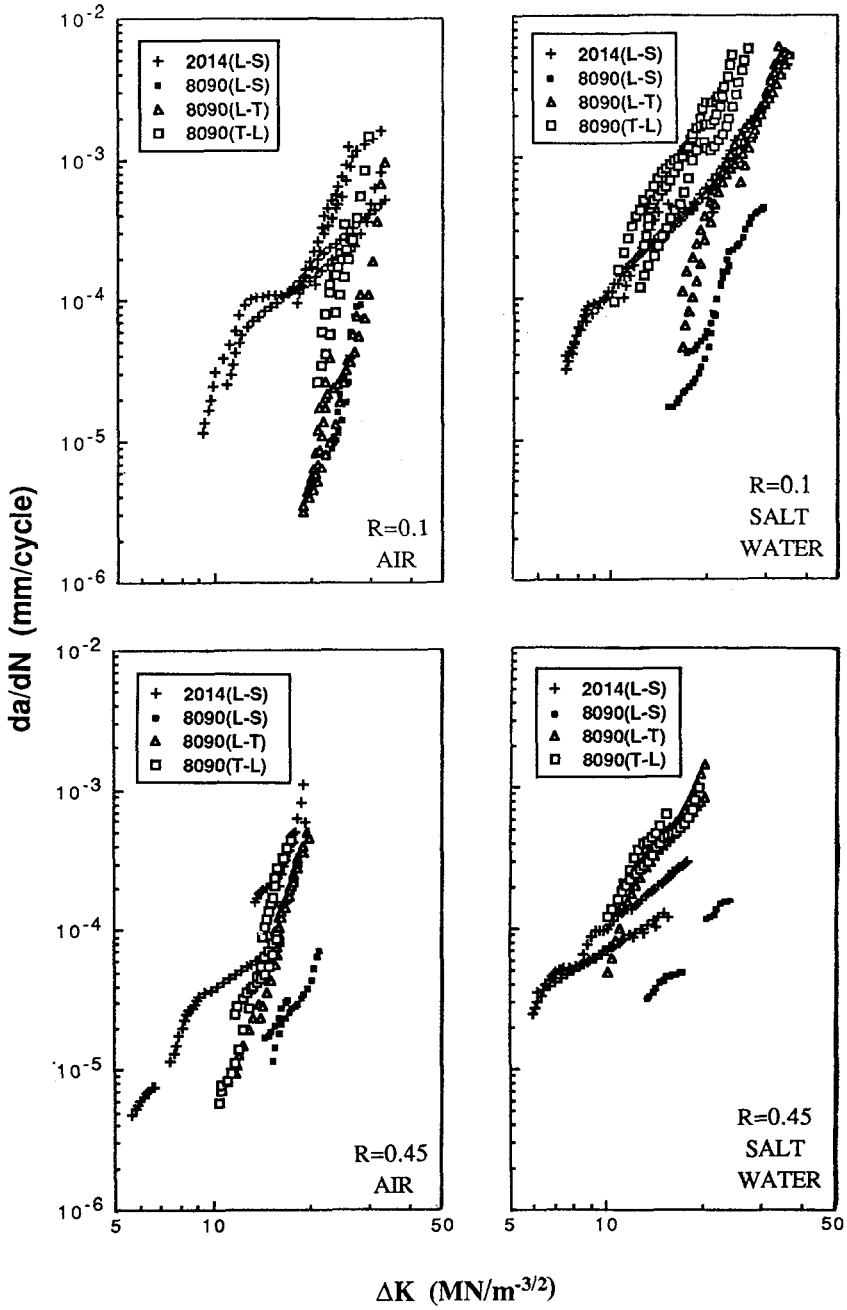

Figure 4: Fatigue crack propagation curves for 8090-T6 and 2014-T6.

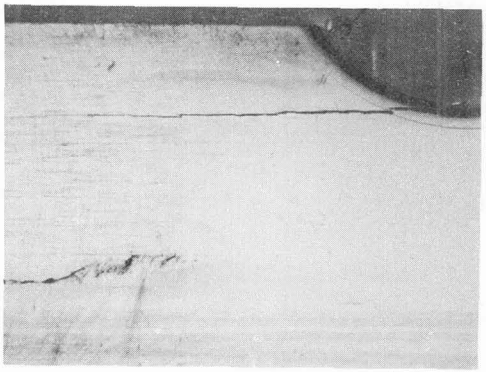

Figure 1: Delamination in 8090 (L-S) specimens without side-grooves.

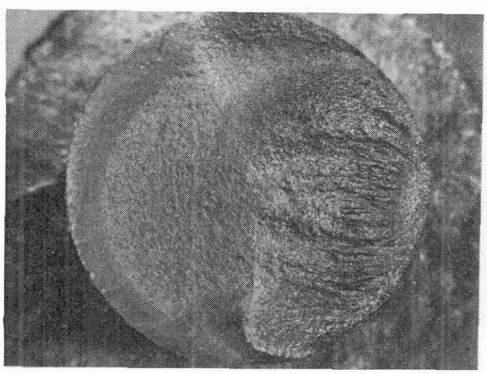

a

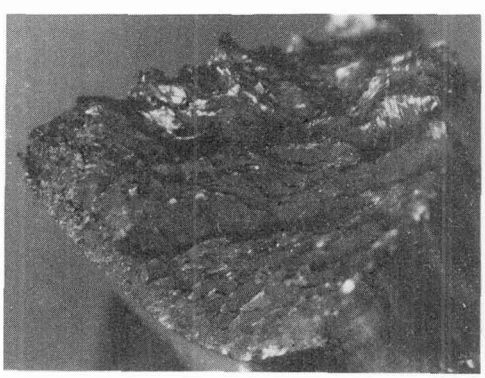

b

Figure 5: Crack growth directions in rotating beam specimens, for 2014 (a) and 8090 (b).

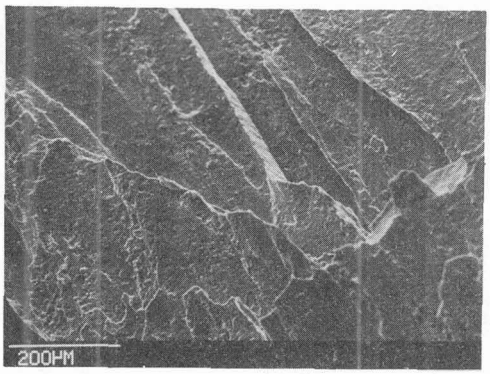

a

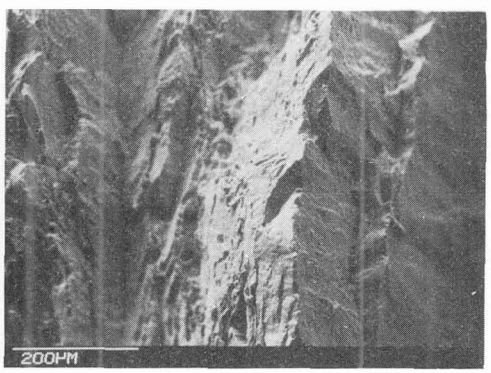

b

Figure 6: Fracture surfaces of 8090 rotating beam specimens.

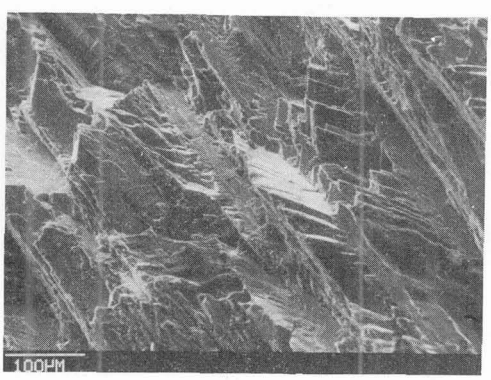

Figure 7: Fracture surface of 8090 fatigue crack propagation specimens.